Triptonide enhances DNA damage by inhibiting TRIP13-mediated DNA repair and synergizes with bortezomib to suppress multiple myeloma

FEN HE[1*], JUNJUN LI[2*], LIJUN PENG[3*], HONGYAN ZHAO[1], MAOYOU LU[1], RUIXIN GAO[1], SIQI WANG[1], YU CHEN[1], RUIHAN TANG[1], ZHENGGUO LI[1], LINLIN ZHANG[1], XINYU ZHANG[1], QIANHAO LI[1], WEIHUI CHEN[1], JIAYU LIU[1], CONG LUO[2], XI ZENG[1] and JILIANG XIA[1]

[1]Hunan Province Key Laboratory of Tumor Cellular and Molecular Pathology, Cancer Research Institute, Hengyang Medical School, University of South China, Hengyang, Hunan 421001, P.R. China; [2]Department of Hematology, The First Affiliated Hospital, Hengyang Medical School, University of South China, Hengyang, Hunan 421001, P.R. China; [3]Department of Spine Surgery, The First Affiliated Hospital, Hengyang Medical School, University of South China, Hengyang, Hunan 421001, P.R. China

Received January 15, 2026; Accepted June 5, 2026

DOI: 10.3892/ijo.2026.5919

Abstract. Multiple myeloma (MM) is a malignant disorder of plasma cells. Combinations of bortezomib (BTZ) with other therapeutic agents remain the mainstay of MM treatment. However, the rising incidence of drug resistance among patients with MM underscores an urgent need for novel therapeutic strategies. The present study identified triptonide (TN), a small-molecule monomer extracted from the traditional Chinese herb *Tripterygium wilfordii* Hook. f., as a synergistic agent that enhanced the anti-MM activity of BTZ, following a screening of 198 compounds from a ubiquitination-focused library. TN effectively inhibited cell proliferation, induced apoptosis, and reduced cell viability in MM cells. Furthermore, the synergistic anti-MM effect between TN and BTZ was validated across MM cell lines, primary MM cells, and xenograft mouse models of MM. Mechanistic investigations revealed that TN synergizes with BTZ by enhancing DNA damage through the suppression of TRIP13-mediated DNA repair pathways, including non-homologous end joining and homologous recombination. Notably, TRIP13 knockdown attenuated TN-induced DNA damage and apoptosis, and diminished the synergistic effect of TN and BTZ on MM cells. Collectively, TN represents a novel anti-MM agent, and the combination of TN with BTZ constitutes a promising therapeutic strategy for the treatment of MM.

Correspondence to: Professor Jiliang Xia, Hunan Province Key Laboratory of Tumor Cellular and Molecular Pathology, Cancer Research Institute, Hengyang Medical School, University of South China, 28 Changshengxi Road, Zhengxiang, Hengyang, Hunan 421001, P.R. China
E-mail: jiliang-xia@usc.edu.cn

*Contributed equally

Key words: multiple myeloma, triptonide, bortezomib, DNA damage, TRIP13

Introduction

Multiple myeloma (MM) is the second most common hematologic malignancy, characterized by the presence of clonally transformed plasma cells in the bone marrow (BM) (1). The combination of bortezomib (BTZ) and other therapeutic agents (2,3), has markedly improved the prognosis of patients with MM. However, the emergence of drug resistance frequently leads to treatment failure and disease relapse (4). Therefore, there is an urgent need to develop novel therapeutic strategies for MM.

Triptonide (TN) is one of the active constituents isolated from the traditional Chinese medicinal herb *Tripterygium wilfordii* Hook. f., with a molecular formula of $C_{20}H_{22}O_6$ and a molecular weight of 358.39 Da (5,6). TN has shown therapeutic potential against various types of cancer, including gastric (7), lung (8), colorectal (9), ovarian (10) and breast cancers (11). Studies demonstrate that TN exerts its anti-cancer effects through multiple mechanisms, such as inhibiting oncogenic pathways (12-14), inducing apoptosis (15), ferroptosis (16) and senescence (17) and promoting endoplasmic reticulum stress (18). Notably, TN acts not only as a monotherapy but also synergizes with other agents, such as oxaliplatin (9) and cisplatin (19). Additionally, TN has demonstrated low toxicity, good oral bioavailability and high efficacy in several studies (6,20). These findings suggest that TN is a promising candidate for cancer treatment. Furthermore, TN reduces thyroid hormone receptor-interacting protein 13 (TRIP13) expression, an AAA+ ATPase involved in chromosome instability (21), protein deubiquitination (22) and DNA repair (23,24), in oral squamous cell carcinoma (25). TRIP13 is overexpressed in patients with MM and linked to BTZ resistance and aggressive disease (22,26,27). Therefore, TN may serve as a promising anti-MM agent by targeting TRIP13.

The present study aimed to evaluate the anti-MM activity of TN and investigated its synergistic effects with BTZ in MM cell lines, primary MM cells, and MM mouse models. It also sought to elucidate the underlying mechanisms by which TN and BTZ synergistically inhibit MM.

Materials and methods

Clinical samples. BM specimens from newly diagnosed patients with MM (n=13), including eight males and five females, were collected at the First Affiliated Hospital of the University of South China (USC), following informed written consent. Specimen collection was between March 2025 and March 2026. The patients' ages ranged from 53-74 years, with a median age of 64.31 years. BM mononuclear cells were purified from specimens using lymphocyte separation medium (Tianjin Haoyang Biological Products Technology Co., Ltd.). Subsequently, $CD138^+$ and $CD138^-$ cells in BM specimens were isolated using CD138 antibody-conjugated magnetic beads (Miltenyi Biotec GmbH). $CD138^+$ and $CD138^-$ cells isolated from BM samples of 11 patients with MM were treated with TN alone; additionally, $CD138^+$ cells isolated from 13 patients with MM were treated with either TN alone or in combination with BTZ. The present study was approved by the Ethics Committee of the USC according to the Declaration of Helsinki (approval no. 20250033). Patient information for MM is included in Table SI.

Cell lines, reagents, and antibodies. Human MM cell lines OCI-My5 and RPMI 8226 were provided by Professor Wen Zhou from the Central South University School of Basic Medical Sciences (Hunan, China). The OCI-My5 and RPMI 8226 cell lines used in the present study have been authenticated by short tandem repeat analysis. MM cells were cultured in RPMI 1640 medium (Zhong Qiao Xin Zhou Biotechnology Co., Ltd.) supplemented with 10% FBS (ExCell Bio). The ubiquitination compound library, TN (cat. no. S9416; purity: 99.81%), and BTZ (cat. no. S1013; purity: 99.97%) were purchased from Selleck Chemicals. Reduced glutathione (GSH; cat. no. T1085), Trolox (cat. no. T1710) and N-acetylcysteine (NAC; cat. no. T0875) were obtained from TargetMol Chemicals Inc. Antibodies against caspase-3 (cat. no. sc-56053; 1:1,000) and γ-H2AX (cat. no. sc-517348; 1:1,000) were purchased from Santa Cruz Biotechnology, Inc. PARP (cat. no. F0148; 1:1,000), DNA-PKcs (cat. no. F1129; 1:1,000) and RAD51 (cat. no. F1110; 1:1,000) antibodies were purchased from Selleck Chemicals. GAPDH (cat. no. 200306-7E4; 1:5,000) and thyroid hormone receptor interactor 13 (TRIP13; cat. no. 240162; 1:1,000) antibodies were obtained from Chengdu Zhengneng Biotechnology Co., Ltd. HRP-conjugated secondary goat anti-rabbit (cat. no. L3012; 1:5,000) and anti-mouse antibodies (cat. no. L3032; 1:5,000) were purchased from Signalway Antibody LLC.

Vectors and transfections. Human *TRIP13* cDNA sequence was amplified and cloned into the pCDH-CMV-MCS-EF1α-GFP vector. Short hairpin (sh) RNAs targeting human *TRIP13* were annealed and ligated into the pLKO-tet-on lentiviral vector. Scrambled shRNA was used as a control. The 2nd generation lentiviral system was applied for virus packaging. Lentiviral particles were packaged by co-transfecting 293T cells (cat. no. CL-0005; Procell Life Science & Technology Co., Ltd.) with the following plasmid DNA: 4 μg pCDH-CMV-MCS-EF1α-GFP-TRIP13 or 4 μg pLKO-tet-on-shRNA, 1 μg pMD2.G, and 3 μg psPAX2, using polyethylenimine (PEI; cat. no. NBS2500; MineBio Life Sciences) as the transfection reagent. After 48 h, the lentivirus was collected and transduced into MM cell lines. Stable TRIP13-overexpressing and TRIP13-knockdown MM cell lines were generated by antibiotic selection: blasticidin S (10 μg/ml; cat. no. ST018; Beyotime Biotechnology) for 6 days and puromycin (1 μg/ml; cat. no. ST551; Beyotime Biotechnology) for 6 days, respectively. All primer sequences are listed in Table SII.

Western blotting. Total cellular proteins were isolated using radioimmunoprecipitation assay (RIPA) lysis buffer (cat. no. P0013B; Beyotime Biotechnology). Protein concentration was determined using a bicinchoninic acid protein assay kit (cat. no. SK1070; Beijing Coolaber Technology Co., Ltd.). Proteins (20 μg per lane) were separated by 10% sodium dodecyl sulfate polyacrylamide gel electrophoresis (SDS-PAGE) and transferred to polyvinylidene fluoride (cat. no. IPFL00010; MilliporeSigma). The membrane was blocked using 5% nonfat dried milk (cat. no. SL1330; Coolaber) in Tris-buffered saline solution containing 0.1% Tween 20 (TBS-T) for 1 h at room temperature and then probed with specific primary antibodies overnight at 4˚C. GAPDH served as the loading control. Subsequently, the membranes were washed with TBS-T, followed by incubating with HRP-conjugated secondary antibodies for 1 h at room temperature, protein bands were visualized using an enhanced chemiluminescence (ECL) western blotting substrate (cat. no. SL1350; Coolaber) and captured with a chemiluminescence imaging system (MiniChemi 610; Beijing Sage Creation Science Co., Ltd.). The grayscale intensity of the protein band was quantified using ImageJ software (1.51j8; National Institutes of Health). Western blotting was performed as previously described (28).

Cell counting kit-8 (CCK-8) assay. MM cells were seeded into 96-well plates (5,000 cells/well) and subjected to CCK-8 (cat. no. K1018; APeXBIO Technology LLC) assay according to the manufacturer's instructions. Cell viability was measured by detecting the absorbance at 450 nm. Each sample was repeated three times.

5-Ethynyl-2'-deoxyuridine (EdU) staining. The EdU staining was performed at 37˚C for 2 h using an EdU experimental kit (cat. no. KTA2031; Abbkine Scientific Co., Ltd.) according to the manufacturer's instructions. Each procedure was repeated three times.

Calcein-AM/PI staining. MM cells were seeded into 96-well plates (5,000 cells/well) and exposed to the indicated pharmacological agents. Subsequently, cells were stained with calcein-AM and propidium iodide (PI) for 30 min at 37˚C using a Calcein-AM/propidium iodide (PI) staining kit (cat. no. KTA1001; Abbkine Scientific Co., Ltd.). Cell viability was quantified as previously described (29). Each procedure was repeated three times.

Comet assay. Comet assays were performed using a Comet Assay® Kit (cat. no. C2041; Beyotime Biotechnology) according to the manufacturer's instructions. Cells ($1x10^5$ cells/ml) were suspended in low-melting-point agarose, and 70 μl of the resulting cell suspension was immediately pipetted onto a microscope slide pre-coated with 1% normal-melting-point agarose. Electrophoresis, neutralization and PI staining were subsequently performed. PI staining was performed for 20 min at room temperature. Comet parameters, including tail length, % tail DNA, and tail moment, were analyzed with CaspLab Comet Assay Software (CASPLab). Each procedure was repeated three times.

Molecular docking and molecular dynamics simulations. First, the three-dimensional structures of TN compounds were retrieved from the PubChem Compound Database (https://pubchem.ncbi.nlm.nih.gov/) and the crystal structure of the human TRIP13 protein was obtained from the Protein Data Bank (https://www.rcsb.org/). Molecular docking and molecular dynamics simulations were performed to analyze the interaction between TN and the TRIP13 protein using Easy2MD (https://github.com/easy2md), an online computational platform, as previously described (30). Binding affinity and binding energy were determined through molecular docking and molecular dynamics simulations, respectively. The strength of the interaction between TN and TRIP13 was assessed based on the binding affinity and binding energy between them.

Non-homologous end joining (NHEJ) and homologous recombination (HR) reporter assay. The efficiency of NHEJ and HR was examined using the HR/NHEJ Reporter Assay kit (Shanghai GeneChem). First, a mutant GFP plasmid containing a specific I-SceI site (DR-GFP) and either the I-SceI-expressing plasmid (pCBASceI) or the NHEJ reporter plasmid (pEJ5-GFP) were transfected into 293T cells using PEI (cat. no. NBS2500; MineBio Life Sciences). After 12 h, the original culture medium was replaced with fresh culture medium containing 500 nM TN. After 24 h, the percentage of GFP-positive cells was assessed by flow cytometry. Each experiment was repeated three times.

Apoptosis assessment by flow cytometry. Cell apoptosis was quantified using the Annexin V-PE/7-AAD Apoptosis Detection kit (cat. no. A213-02; Vazyme Biotech Co., Ltd.) according to the manufacturer's instructions. Cells were stained with Annexin V-PE (labeled apoptotic cells) and 7-AAD (labeled dead cells) for 10 min at room temperature, then analyzed on an LSR II flow cytometer (BD Biosciences) and gated in FlowJo V10 (BD Biosciences). The apoptotic cells include the early apoptotic cells (Annexin V+, 7-AAD-) and late apoptotic cells (Annexin V+, 7-AAD+). Each test was repeated three times.

Reverse transcription-quantitative (RT-q) PCR. Total RNA was extracted from $1x10^6$ cells using RNA isolater (cat. no. R401-01-AA; Vazyme Biotech Co., Ltd.) and then retrotranscribed using the RevertAid First Strand cDNA Synthesis Kit (cat. no. K1621; Thermo Fisher Scientific, Inc.) according to the manufacturer's instructions. qPCR was performed using SYBR qPCR Master Mix (cat. no. Q311; Vazyme Biotech Co., Ltd.). The qPCR process was run on the Archimed R4 qPCR System (Thermo Fisher Scientific). The PCR cycling conditions were: Initial denaturation at 95˚C for 30 sec; followed by 40 cycles of denaturation at 95˚C for 10 sec, annealing and extension at 60˚C for 30 sec. Fluorescence intensity was detected after each cycle. Fold changes were calculated using the $2^{-\Delta\Delta Cq}$ method and *ACTIN* mRNA as a reference, following established protocols described in a previous publication (31). Primer sequences are listed in Table SII. Each experiment was repeated 3 times.

RNA sequencing. Total RNA was extracted from RPMI 8226 cells treated with or without TN, using TRIzol® reagent (Thermo Fisher Scientific, Inc.). The following procedures were carried out by Wuhan SeqHealth Tech Co., Ltd. RNA quality was evaluated, and samples with high integrity were selected. After rRNA depletion, mRNA was fragmented and reverse-transcribed into cDNA. Sequencing libraries were constructed via adapter ligation and PCR amplification. Finally, library sequencing was performed on the Illumina platform (Illumina, Inc.) using the paired-end mode. Differentially expressed genes were identified using thresholds of fold change >1.5 and P-value <0.05. Subsequently, functional enrichment analyses were conducted by online software DIVID (https://davidbioinformatics.nih.gov/) based on differentially expressed genes.

The analysis of gene expression profiling data. RNA sequencing was Gene expression profile (GEP) data was obtained from NIH Gene Expression Omnibus (GEO) database (https://ncbi.nlm.nih.gov/geo/). GEP data (GSE6477; https://www.ncbi.nlm.nih.gov/geo/query/acc.cgi?acc=GSE6477) includes 15 healthy subjects, 73 newly diagnosed MM patients, and 28 relapsed MM patients. The expression of *TRIP13* was investigated in those samples.

Animal experiments. A total of 12 eight-week-old female NOD/ShiLtJGpt-Prkdcem26Cd52Il2rgem26Cd22/Gpt (NCG) mice (GemPharmatech Co. Ltd.) were used in the present study. The average weight of mice was ~21.5±0.53 g. All mice were maintained under SPF conditions in a controlled environment of 20-22˚C, with a 12-h light/dark cycle and 50-70% humidity. OCI-My5 cells were subcutaneously injected into the right flank of 12 NCG mice ($5x10^6$ cells/mouse). At nine days following injection of MM cells, these mice were randomly divided into four groups and treated with saline (administered intraperitoneally), BTZ (0.5 mg/kg; administered intraperitoneally), TN (2.5 mg/kg; administered intraperitoneally), or the combination group (0.5 mg/kg BTZ and 2.5 mg/kg TN; administered intraperitoneally). Concurrently, tumor volume and diameter were measured in mice using digital caliper every three days. Tumor volume was calculated using the formula: volume=(length x width^2)/2. At 24 days following injection of MM cells, the final tumor measurement was performed. Subsequently, 24 h after the last measurement, mice were humanely sacrificed with CO_2 at a volume displacement rate of 50% chamber volume per minute and tumors were surgically excised. Images of

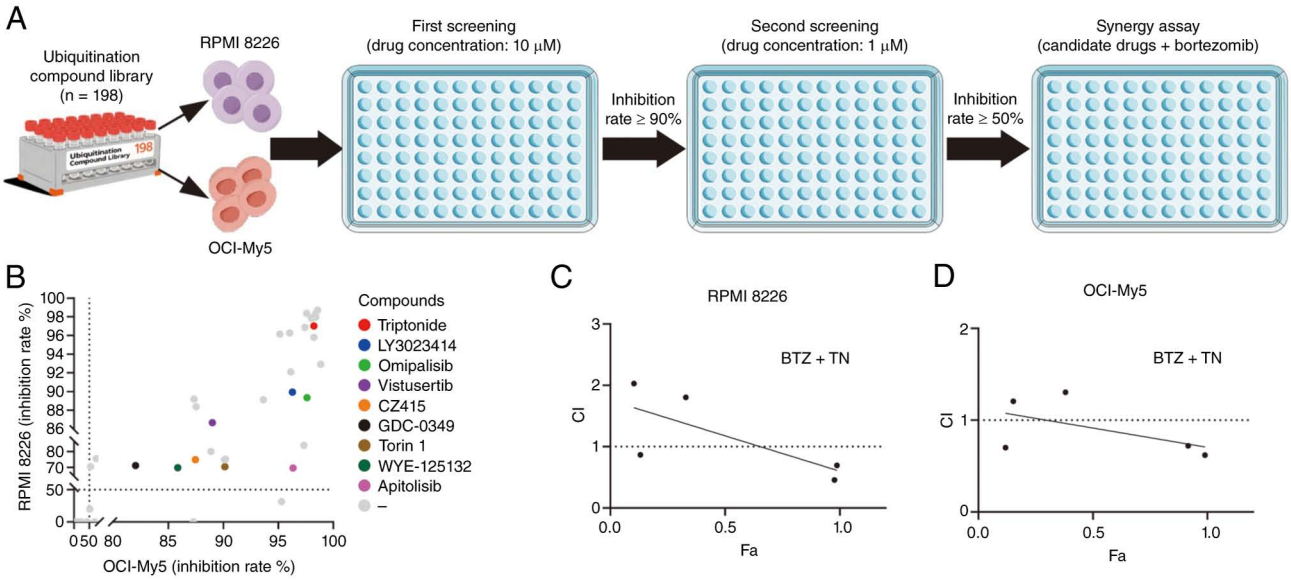

Figure 1. Identification of synergy between TN and BTZ in MM cells through screening ubiquitination compound library. (A) The model for screening the ubiquitination compound library. (B) The nine candidate agents, which demonstrated at ≥50% inhibitory efficacy in both RPMI 8226 and OCI-My5 cells at a concentration of 1 μM, were identified through two rounds of screening. The CI values of TN with BTZ in (C) RPMI 8226 and (D) OCI-My5 cells were analyzed using the Chou-Talalay method. A CI value <1 indicates a synergistic effect. TN, triptonide; BTZ, bortezomib; MM, multiple myeloma; CI, combination index.

the excised tumors were immediately captured and the excised tumors processed for western blotting and immunohistochemical (IHC) analysis. The maximum allowable tumor volume and diameter are 2,000 mm^3 and 20 mm, respectively. The maximal tumor size was not exceeded in the present study. The animal study was performed in accordance with the guidelines of the Institutional Animal Care and Use Committee and the Local Veterinary Office, and was approved by the Ethics Committee of the USC (approval no. USC2024XS052).

IHC. IHC staining was conducted using M&R HRP/DAB Detection IHC Kit (cat. no. HC301; Vazyme Biotech Co., Ltd.) according to the manufacturer's instructions. Briefly, 4-μm tumor sections were deparaffinized in xylene, rehydrated in graded ethanol, and subjected to antigen retrieval in sodium citrate buffer (pH 6.0) under high pressure. Endogenous peroxidase was blocked with hydrogen peroxide blocking reagent (from IHC kit) for 20 min at room temperature. Sections were permeabilized with 0.5% Triton X-100 for 10 min at room temperature, then incubated overnight at 4˚C with primary antibodies: Ki-67 (cat. no. 9027T; Cell Signaling Technology; 1:100), γ-H2AX (cat. no. 83307-2-RR; Proteintech Group, Inc.; 1: 2,000), cleaved caspase-3 (cat. no. 9661; Cell Signaling Technology, Inc.; 1:400), and TRIP13 (cat. no. 240162; Zenbio; 1:100). Subsequently, HRP polymer (from IHC kit) was applied for 20 min at room temperature, followed by DAB substrate solution (from IHC kit) to generate a chromogenic signal. Nuclei were counterstained with hematoxylin (cat. no. C140; Applygen Technologies, Inc.) for 3 min at room temperature. The stained sections were examined under a bright-field light microscope (ECLIPSE E200; Nikon Corporation). Images were acquired at 400x magnification using Motic Images Plus 2.0 system (Motic Instruments).

Statistical analysis. All data are presented as mean ± standard deviation (SD). Data that followed a normal distribution were analyzed using two-sided t-test or one-way analysis of variance (ANOVA) followed by Tukey's test. For data that did not follow a normal distribution, nonparametric statistical methods, including Wilcoxon matched-pairs signed rank test, Mann-Whitney test and KruskalWallis H test followed by Dunn's multiple comparisons test, were employed. Data analysis was performed using GraphPad Prism 7 (Dotmatics). $P<0.05$ was considered to indicate a statistically significant difference.

Results

Compound screening identifies synergistic effects between TN and BTZ in MM cells. To identify novel anti-MM strategies, the present study screened 198 compounds from a ubiquitination-targeted compound library in MM cell lines (Fig. 1A). In the primary screen, each compound was applied at 10 μM to RPMI 8226 cells, followed by CCK-8 assays to assess viability. Compounds showing >90% inhibition were further tested in OCI-My5 cells. 55 compounds exhibited over 90% inhibition in both RPMI 8226 and OCI-My5 cells (Table SIII). To prioritize more potent candidates, these 55 compounds were retested at 1 μM in a secondary screen. As shown in Fig. 1B and Table SIV, 29 compounds maintained ≥50% inhibitory activity in both cell lines, with nine representing promising new therapeutic candidates for MM.

BTZ, a reversible proteasome inhibitor, is a first-line clinical drug for MM (32). Recently, combinations of BTZ with other agents have improved the prognosis of patients with MM (2,33). However, most patients relapse due to drug resistance (34). To identify novel therapeutic strategies, the present study evaluated the synergistic effects of BTZ combined with nine candidate compounds in MM cells. First, their IC_{50} (half-maximal inhibitory concentration) values were

determined in MM cells (Fig. S1A). To evaluate synergy, RPMI 8226 cells were treated with different doses of BTZ and each compound alone or in combination, followed by CCK-8 assays (Fig. S1B). Combination index (CI) values were calculated using the Chou-Talalay method, with CI <1 indicating synergy (35). Among all combination regimens, BTZ plus TN exhibited the strongest synergistic effect (Fig. 1C). This synergy was also observed in OCI-My5 cells (Fig. 1D). These findings suggest that the combination of BTZ and TN synergistically inhibits MM cell proliferation.

TN effectively suppresses cell proliferation and induces apoptosis and cell death in MM cells. TN has exhibited anti-tumor activity in various types of cancer. To assess its effect on MM cell proliferation, MM cells were treated with TN, followed by CCK-8 assays, colony formation, EdU staining and cell cycle assays. TN markedly reduced cell number (Fig. 2A), inhibited colony formation in OCI-My5 cells (Fig. 2B), and decreased the proportion of EdU-positive cells in both MM cell lines (Fig. 2C). Furthermore, TN increased the proportion of cells in G0/G1 phase while reducing those in S and G_2/M phases (Fig. S2A), indicating blockade of G_0/G_1-to-S progression. These results demonstrated that TN effectively suppresses MM cell proliferation.

TN has been shown to induce apoptosis in ovarian cancer (10), breast cancer (36), and acute myeloid leukemia (13). To determine whether TN induces apoptosis in MM cells, RPMI 8226 and OCI-My5 cells were treated with TN and apoptosis levels were assessed by flow cytometry and western blotting. Flow cytometry revealed a significant increase in apoptotic cells in both MM cell lines upon TN treatment (Fig. 2D). Consistently, TN markedly elevated the levels of cleaved caspase-3 and poly ADP-ribose polymerase (PARP), well-established apoptosis markers (37), in both MM cell lines (Fig. 2E). Calcein-AM/PI staining further showed that TN markedly reduced MM cell viability (Fig. 2F). Notably, primary $CD138^+$ MM cells were more sensitive to TN than paired $CD138^-$ non-MM cells from the same patients with MM (Fig. 2G). Additionally, TN showed minimal inhibition of the human B-cell line GM12878 at the same doses used for MM cells, with most cells remaining viable even at high concentrations (Fig. S2B). These results indicate that TN represents a promising targeted agent for MM treatment.

TN and BTZ synergistically inhibit cell proliferation, increase apoptosis, and induce cell death in MM cells. To confirm the synergistic effect of TN and BTZ in MM cells, RPMI 8226 and OCI-My5 cells were treated with TN and BTZ alone or in combination, followed by CCK-8 assays, colony formation and EdU staining to assess proliferation. The CCK-8 results showed that the combination markedly reduced cell numbers compared to either agent alone (Fig. 3A). TN and BTZ also synergistically decreased colony formation in OCI-My5 cells (Fig. 3B). The proportion of EdU-positive cells was markedly lower in combination-treated cells than in those receiving single-agent treatment (Fig. 3C). These results demonstrate that TN and BTZ synergistically inhibit MM cell proliferation.

TN and BTZ are both capable of inducing apoptosis in MM cells; therefore, the present study investigated whether their combination synergistically increased the proportion of apoptotic cells. Flow cytometry showed that the combination of TN and BTZ markedly increased apoptosis levels in both MM cell lines compared to treatment with either agent alone (Fig. 3D). Consistently, cleaved caspase-3 and PARP levels were higher in cells treated with both drugs than with either drug alone, surpassing those from high-dose monotherapy (Fig. S3). Additionally, the results of Calcein-AM/PI staining showed markedly reduced viability in MM cell lines treated with TN plus BTZ compared to either drug alone (Fig. 3E and 3F). Notably, the combination synergistically reduced viability in primary MM cells from thirteen newly diagnosed patients (Fig. 3G). Therefore, TN and BTZ exert a strong synergistic effect in MM cells.

TN acts synergistically with BTZ to augment DNA damage by inhibiting DNA repair. To investigate how TN inhibits MM cells, the present study performed RNA sequencing on RPMI 8226 cells treated with or without TN. This revealed 1,458 differentially expressed genes (fold change >1.5; $P<0.05$; Table SV; Fig. 4A). Gene enrichment analysis indicated TN impairs the DNA damage response (Fig. 4B). Consistently, γ-H2AX, a marker of double-strand breaks (DSBs) (38), increased in TN-treated MM cells (Fig. 4C), and comet assays showed longer comet tails, confirming elevated DNA damage (Fig. 4D). Since DSBs can arise from oxidative stress, telomere shortening, or defective DNA repair (39), each mechanism was tested. Antioxidants (Trolox, GSH, NAC) failed to rescue TN-induced cell death or γ-H2AX upregulation (Fig. S4A-C), excluding oxidative stress. Telomere length, assessed by T/S ratio (40), remained unchanged after TN treatment (Fig. S4D), ruling out telomere shortening. Instead, TN markedly reduced DNA-PKcs and RAD51 protein levels, key regulatory proteins involved in NHEJ and HR (38), respectively (Fig. 4E), and GFP-reporter assays confirmed suppression of both NHEJ and HR repair (Fig. 4F). Together, these showed that TN enhanced DNA damage in MM cells by inhibiting DNA repair.

Consistent with a previous study (41), BTZ induced oxidative stress and DNA damage in MM cells (Fig. S4E and F), supporting synergy with TN in amplifying DNA damage. Western blotting confirmed that TN + BTZ increased γ-H2AX more than either drug alone, even at high doses (Fig. 4G). Comet assays showed longer tails with the combination versus monotherapy (Fig. 4H), further validating synergistic DNA damage. Since DNA damage directly inhibits proliferation and triggers apoptosis, it likely underlies the synergistic anti-MM effect of TN and BTZ.

TN interacts with TRIP13 and downregulates its expression levels in MM cells. TN has been reported to reduce TRIP13 expression in oral squamous cell carcinoma cells (25). TRIP13 is an AAA+ ATPase involved in both NHEJ and HR DNA repair (23,24). Analysis of the Gene Expression Omnibus (GEO) database (GSE6477) showed higher TRIP13 mRNA levels in MM cells from newly diagnosed patients compared with healthy donor plasma cells, with further elevation at relapse (Fig. 5A). TRIP13 was also highly expressed in RPMI 8226 and OCI-My5 MM cells but low in GM12878 control cells (Fig. 5B). TN markedly downregulated TRIP13 at both mRNA and protein levels in these MM lines (Fig. 5C and D). Given TN's selective anti-MM activity, TRIP13 probably mediates this selectivity. Additionally, the present study

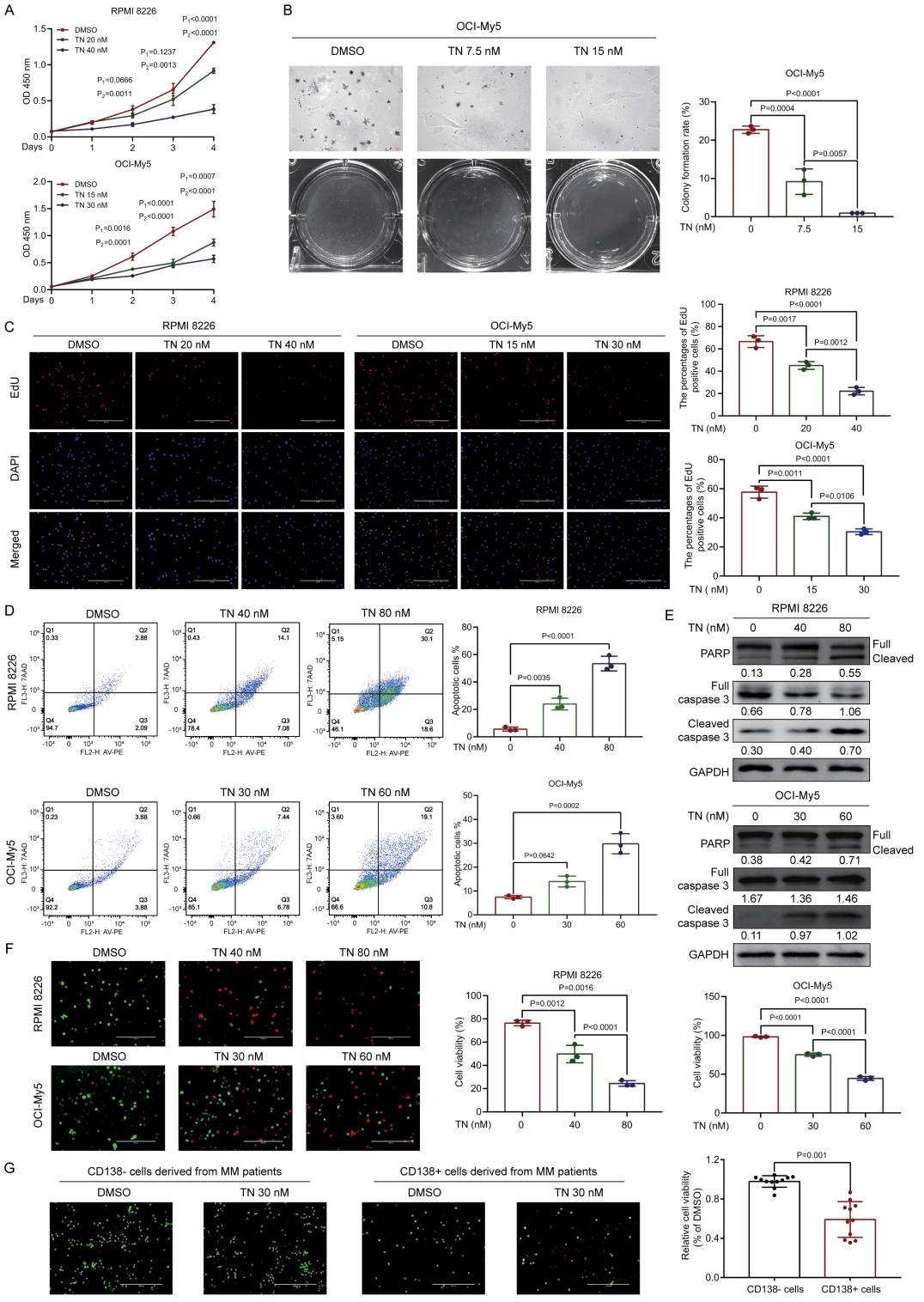

Figure 2. TN effectively inhibits MM cells. (A) Growth curves of MM cells treated with or without TN. p_1=0.0666, p_1=0.1237, p_1<0.0001 DMSO vs. TN (20 nM); p_2=0.0011, p_2=0.0013, p_2<0.0001 DMSO vs. TN (40 nM) in RPMI 8226 cells. p_1=0.0016, p_1<0.0001, p_1=0.0007 DMSO vs. TN (15 nM); p_2=0.0001, p_2<0.0001, p_2<0.0001 DMSO vs. TN (30 nM) in OCI-My5 cells. (B) Clonogenic analysis of OCI-My5 treated with or without TN. P=0.0004 control vs. TN (7.5 nM); P<0.0001 control vs. TN (15 nM); P=0.0057 of TN (7.5 nM vs. 15 nM). Scale bar, 100 μm. (C) MM cells were treated with or without TN for 48 h, followed by 5-Ethynyl-2'-deoxyuridine staining. P=0.0017 control vs. TN (20 nM); P<0.0001 control vs. TN (40 nM); P=0.0012 of TN (20 nM vs. 40 nM) in RPMI 8226 cells. P=0.0011 control vs. TN (15 nM); P<0.0001 of control vs. TN (30 nM); P=0.0106 TN (15 nM vs. 30 nM) in OCI-My5 cells. Scale bar, 200 μm. (D) Assessment of apoptosis by using Annexin V-PE/7-AAD staining in MM cells treated with or without TN for 48 h. P=0.0035 control vs. TN (40 nM); P<0.0001 control vs. TN (80 nM) in RPMI 8226 cells. P=0.0642 of control vs. TN (30 nM); P=0.0002 of control vs. TN (60 nM) in OCI-My5 cells. (E) Western blot analysis of PARP, caspase 3, and GAPDH in RPMI 8226 and OCI-My5 cells treated with or without TN for 48 h. (F) Cell viability was assessed by Calcein-AM/PI staining in MM cells treated with or without TN for 48 h. Viable cells were labeled with Calcein-AM (green) and dead cells were labeled with PI (red). P=0.0012 control vs. TN (40 nM); P=0.0016 control vs. TN (80 nM); P<0.0001 TN (40 nM vs. 80 nM) in RPMI 8226 cells. P<0.0001 TN (30 nM) or TN (60 nM) vs. control, TN (30 nM) vs. TN (60 nM) in OCI-My5 cells. Scale bar, 200 μm. (G) Cell viability of primary $CD138^-$ and $CD138^+$ cells derived from the same patients with MM (n=11) following treatment with or without TN. P=0.001 of $CD138^-$ cells vs. $CD138^+$ cells. Scale bar, 200 μm. n=3 independent experiments in (A-D and F). Statistical significance was assessed using one-way ANOVA followed by Tukey's honestly significant difference test in (A-D and F); a Wilcoxon matched-pairs signed rank test was applied in (G). TN, triptonide; BTZ, bortezomib; MM, multiple myeloma.

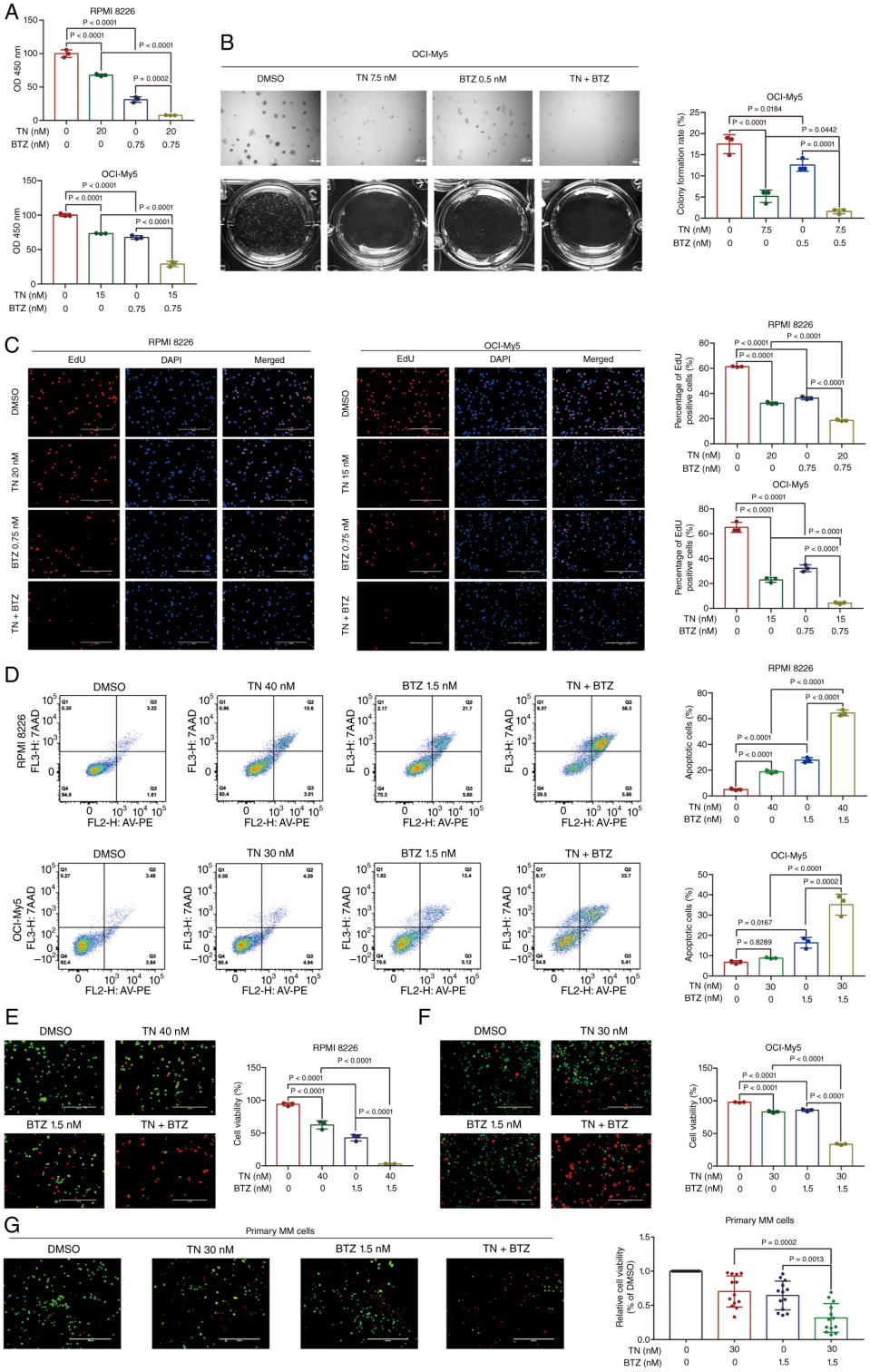

Figure 3. The combination of TN and BTZ synergistically inhibits MM cells. (A) CCK-8 assays of MM cells treated with TN and BTZ in alone or in combination for 48 h. P<0.0001 control vs. TN (20 nM); P<0.0001 control vs. BTZ (0.75 nM), TN vs. TN + BTZ; P=0.0002 of BTZ vs. TN + BTZ in RPMI 8226 cells. P<0.0001 of TN (15 nM) or BTZ (0.75 nM) vs. control, TN vs. TN + BTZ, and BTZ vs. TN + BTZ in OCI-My5 cells. (B) Clonogenic analysis of OCI-My5 treated with TN alone or in combination with BTZ. P<0.0001 control vs. TN (7.5 nM); P=0.0184 control vs. BTZ (0.5 nM); P=0.0442 TN vs. TN + BTZ; P=0.0001 BTZ vs. TN + BTZ. Scale bar, 100 μm (C) 5-Ethynyl-2'-deoxyuridine staining of MM cells treated with TN and BTZ alone or in combination for 48 h. P<0.0001 of TN (20 nM) or BTZ (0.75 nM) vs. control, TN + BTZ vs. control, BTZ vs. TN + BTZ in RPMI 8226 cells. P<0.0001 control vs. TN (15 nM), control vs. BTZ (0.75 nM), BTZ vs. TN + BTZ, P=0.0001 of TN vs. TN + BTZ in OCI-My5 cells. Scale bar, 200 μm. (D) MM cells were treated with TN and BTZ alone or in combination for 48 h, followed by assessment of apoptosis using flow cytometry. P<0.0001 of TN (40 nM) or BTZ (1.5 nM) vs. control, TN vs. TN + BTZ, BTZ vs. TN + BTZ in RPMI 8226 cells. P=0.8289 of control vs. TN (30 nM); P=0.0167 control vs. BTZ (0.75 nM); P<0.0001 of TN vs. TN + BTZ; P=0.0002 of BTZ vs. TN + BTZ in OCI-My5 cells. (E and F) MM cells were treated with TN and BTZ alone or in combination for 48 h, followed by examination of cell viability using Calcein-AM/PI staining. P<0.0001 control vs. TN (40 nM), control vs. BTZ (1.5 nM), BTZ vs. TN + BTZ, and TN vs. TN + BTZ in RPMI 8226 cells. P<0.0001 control vs. TN (30 nM), control vs. BTZ (1.5 nM), TN vs. TN + BTZ, BTZ vs. TN + BTZ in OCI-My5 cells. Scale bar, 200 μm. (G) Cell viability assay of CD138$^+$ cells derived from patients with MM (n=13) by using Calcein-AM/PI staining. P=0.0002 TN (30 n M) vs. TN + BTZ; P=0.0013 of BTZ (1.5 nM) vs. TN + BTZ. Scale bar, 200 μm. n=3 independent experiments in (A-F). Statistical significance was assessed using one-way ANOVA followed by Tukey's honestly significant difference test in (A-G). TN, triptonide; BTZ, bortezomib; MM, multiple myeloma.

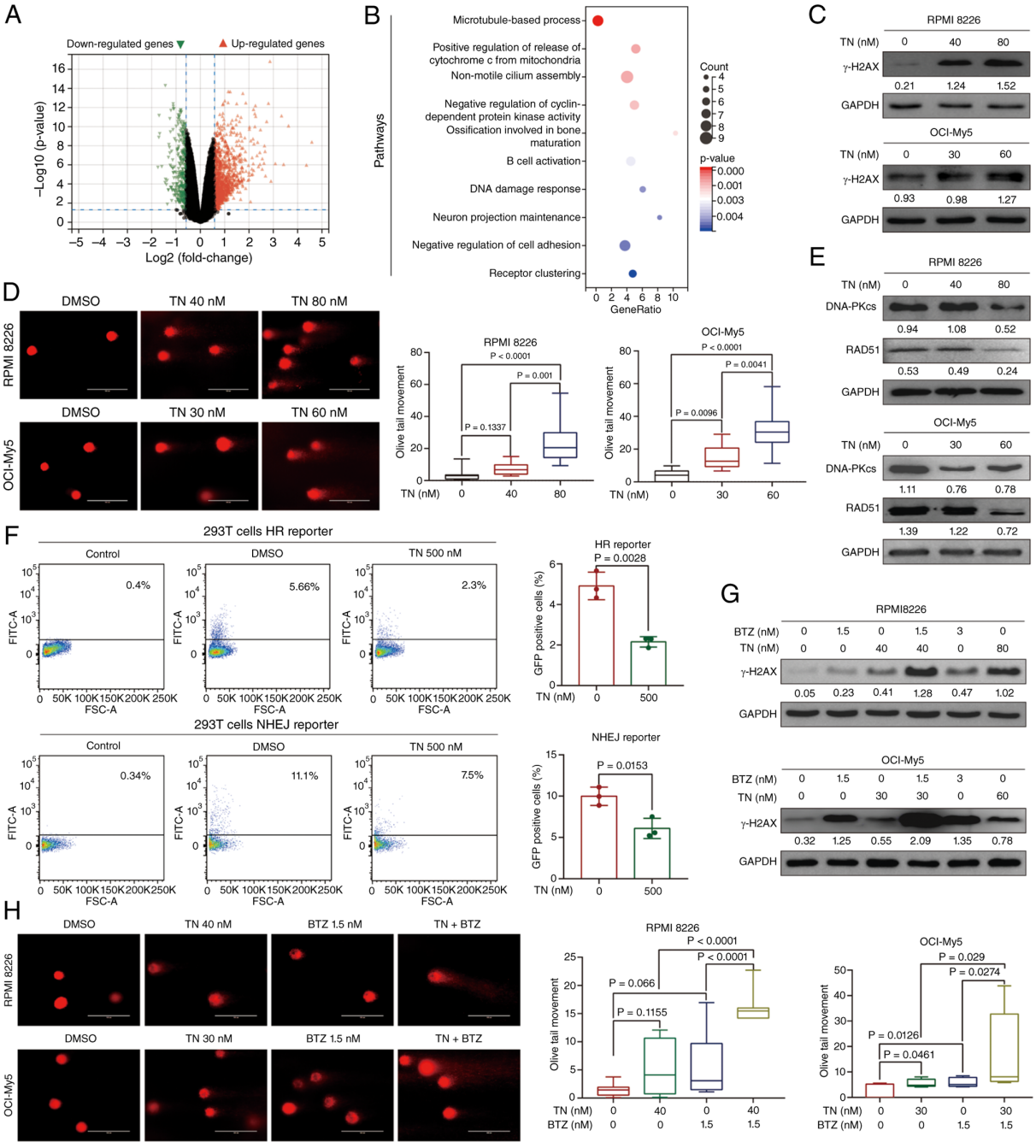

Figure 4. TN synergizes with BTZ to enhance DNA damage through inhibiting DNA repair. (A) The volcano map of gene profiling between RPMI 8226 cells treated with or without TN (40 nM) for 24 h. (B) Pathway enrichment analysis based on the differently expressed genes between TN treated RPMI 8226 cells and control cells. (C) Western blot analysis of γ-H2AX and GAPDH expression in MM cells treated with TN (0, 40 nM, 80 nM in RPMI 8226; 0, 30 nM. 60 nM in OCI-My5) for 24 h. (D) Analysis of DNA damage by comet assay in MM cells treated with TN for 24 h. P=0.1337 control vs. TN (40 nM); P<0.0001 control vs. TN (80 nM); P=0.001 of TN (40 nM) vs. TN (80 nM) in RPMI 8226 cells. P=0.0096 control vs. TN (30 nM); P<0.0001 control vs. TN (60 nM); P=0.0041 of TN (30 nM) vs. TN (60 nM) in OCI-My5 cells. Scale bar, 100 μm. (E) Western blot analysis of expression DNA-PKcs, RAD51 and GAPDH in MM cells treated with TN (0, 40 nM, 80 nM in RPMI 8226; 0, 30 nM. 60 nM in OCI-My5) for 24 h. (F) HR and NHEJ repair efficiency in 293T cells treated with or without TN was assessed by flow cytometry. The percentage of GFP-positive cells was used to indicate the capacity for HR and NHEJ repair. P=0.0028, P=0.0153 of control vs. TN (500 nM) in HR reporter and NHEJ reporter, respectively. (G) Western blot analysis of γ-H2AX and GAPDH expression in MM cells treated with TN (40 nM in RPMI 8226; 30 nM in OCI-My5) and BTZ (1.5 nM) alone or in combination for 24 h. (H) MM cells were treated with TN and BTZ alone or in combination for 24 h, followed by DNA damage assessment using comet assay. P=0.1155 control vs. TN (40 nM); P=0.066 control vs. BTZ (1.5 nM); P<0.0001 of TN vs. TN + BTZ and BTZ vs. TN + BTZ in RPMI 8226 cells. P=0.881 control vs. TN (30 nM); P=0.8892 of control vs. BTZ (1.5 nM); P=0.0466 TN vs. TN + BTZ; P=0.025 of BTZ vs. TN + BTZ in OCI-My5 cells. Scale bar, 100 μm. n=3 independent experiments in (F). Statistical significance was assessed using the Kruskal-Wallis H test followed by Dunn's multiple comparisons test in (D and H); an unpaired two-sided t-test was used in (F). TN, triptonide; BTZ, bortezomib; MM, multiple myeloma; HR, homologous recombination; NHEJ, non-homologous end joining.

investigated the interaction between TN and TRIP13 proteins through molecular docking and molecular dynamics simulations using easy2MD, an online computational platform. A binding affinity below -5 kcal/mol and a binding energy below -15 kJ/mol are generally indicative of a strong and stable interaction. The analysis results revealed strong binding of TN

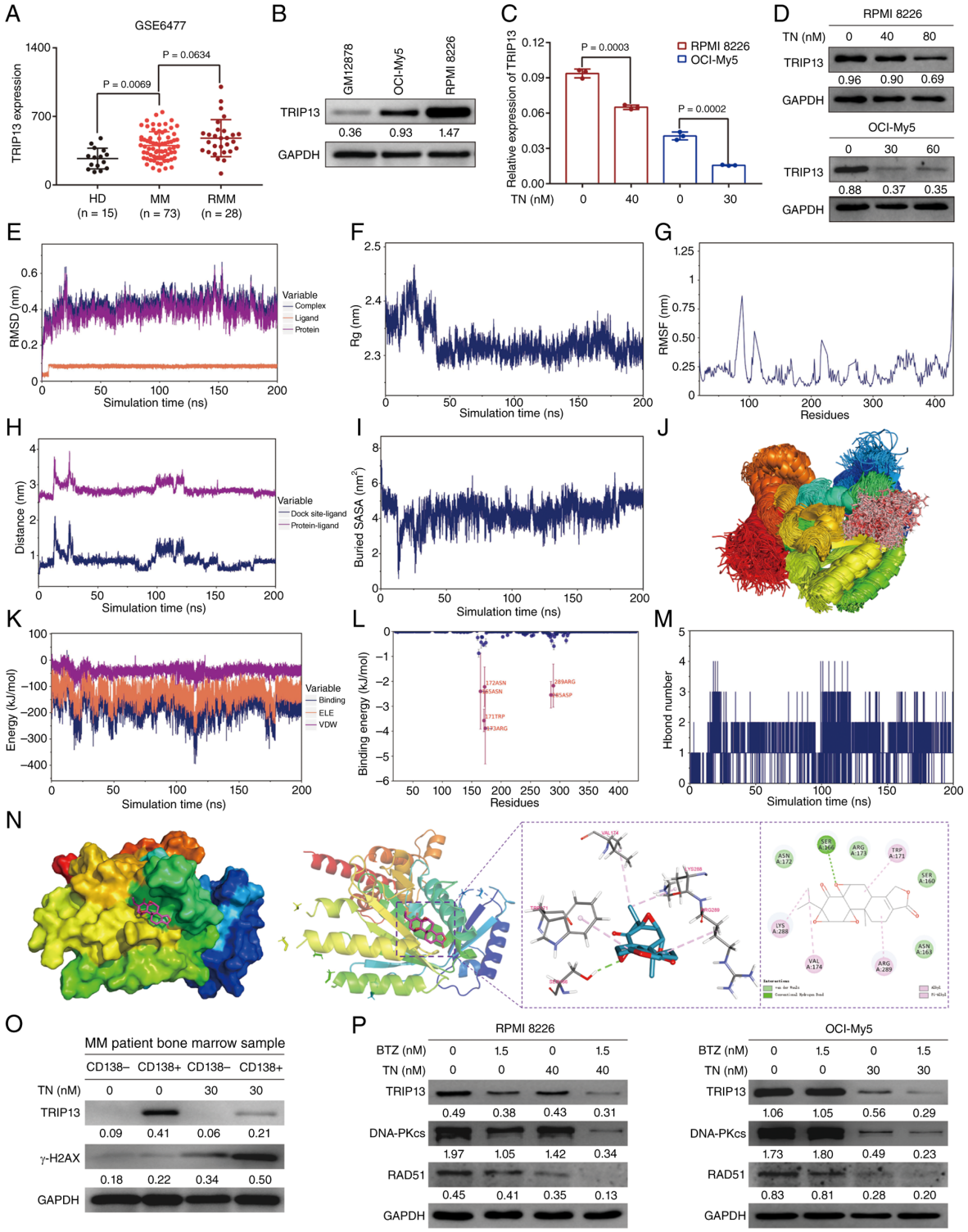

Figure 5. TN interacts with TRIP13 and reduces its expression in MM cells. (A) Expression levels of *TRIP13* mRNA in primary MM cells from newly diagnosed patients with MM (n=73) and relapsed patients with MM (n=28), as well as in plasma cells from healthy donors (n=15), were analyzed using GEO database dataset GSE6477. P=0.0069 of HD vs. MM. P=0.0634 of MM vs. RMM. (B) Western blot analysis of TRIP13 and GAPDH expression in GM12878, OCI-My5, and RPMI 8226 cells. (C) quantitative PCR of *TRIP13* in MM cells treated with or without TN for 24 h. P=0.0003 control vs. TN (40 nM) in RMPI 8226 cells. P=0.0002 control vs. TN (30 nM) in OCI-My5 cells. (D) Western blot analysis of TRIP13 and GAPDH expression in MM cells treated with or without TN (40 nM, 80 nM in RPMI 8226, 30 nM, 60 nM in OCI-My5) for 24 h. (E) RMSD of the complex, TRIP13 protein, and TN. (F) Rg of the complex. (G) RMSF of the TRIP13 protein within the complex. (H) Docking site-ligand interaction (Dock site-ligand). (I) Buried SASA between TN and TRIP13 protein. (J) Overlay of simulated conformations. (K) Binding energy between TN and TRIP13 proteins, including VDW and ELE components. (L) Contribution of amino acids to binding energy. (M) Number of hydrogen bonds. (N) Interaction of TRIP13 protein with TN. (O) Western blot analysis of TRIP13, γ-H2AX, and GAPDH expression in $CD138^+$ and $CD138^-$ primary cells isolated from MM patient, with or without treatment with TN (30 nM). (P) Western blot analysis of TRIP13, DNA-PKcs, RAD51 and GAPDH expression in MM cells treated with TN (40 nM in RPMI 8226; 30 nM in OCI-My5) and BTZ (1.5 nM) alone or in combination. n=3 independent experiments in (C). Statistical significance was assessed using the Kruskal-Wallis H test followed by Dunn's multiple comparisons test in (A); an unpaired two-sided t-test was used in (C). TN, triptonide; MM, multiple myeloma; RMM, relapsed multiple myeloma; GEO, Gene Expression Omnibus; RMSD, Root Mean Square Deviation; Rg, Radius of Gyration; RMSF, Root Mean Square Fluctuation; SASA, Solvent Accessible Surface Area; VDW, van der Waals; ELE, electrostatic.

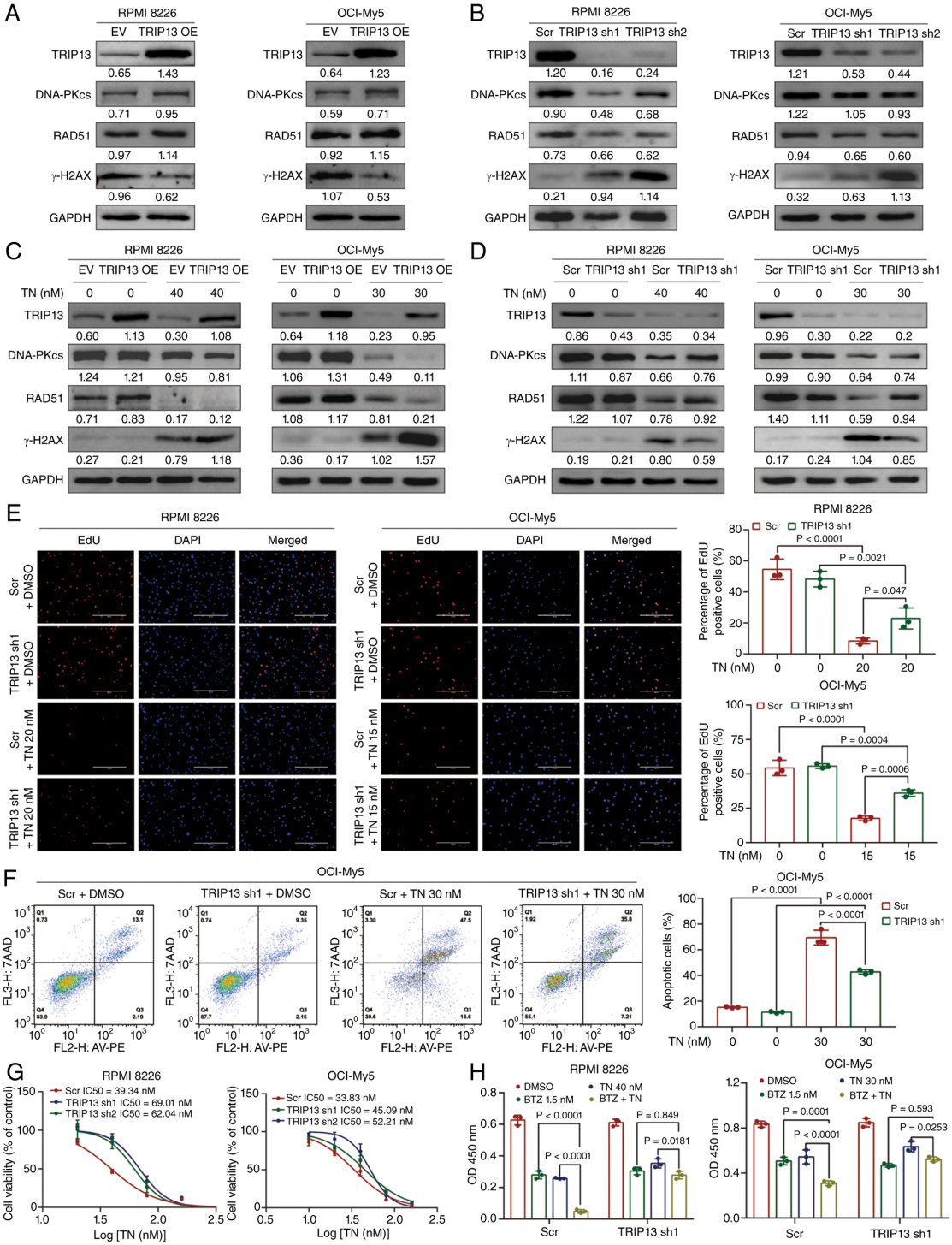

Figure 6. TN enhances DNA damage by inhibiting TRIP13-mediated DNA repair, thereby synergizing with BTZ. (A) Western blot analysis of TRIP13, DNA-PKcs, RAD51, γ-H2AX, and GAPDH expression in RPMI 8226 and OCI-My5 cells with EV or TRIP13-OE. (B) Western blot analysis of TRIP13, DNA-PKcs, RAD51, γ-H2AX and GAPDH expression in RPMI 8226 and OCI-My5 cells with Scr, TRIP13-sh1 and TRIP13-sh2. (C) Western blot analysis of TRIP13, DNA-PKcs, RAD51, γ-H2AX and GAPDH expression in MM cells with EV or TRIP13-OE treated with or without TN (40 nM in RPMI 8226; 30 nM in OCI-My5) for 24 h. (D) Western blot analysis of TRIP13, DNA-PKcs, RAD51, γ-H2AX and GAPDH expression in MM cells with Scr or TRIP13-sh1 treated with or without TN (40 nM in RPMI 8226; 30 nM in OCI-My5) for 24 h. (E) EdU staining of MM cells with Scr or TRIP13-sh1 treated with or without TN (20 nM in RPMI 8226; 15 nM in OCI-My5) for 48 h. P<0.0001 scr vs. TN treated scr; P=0.0021 of TRIP13-sh1 vs. TN treated TRIP13-sh1; P=0.047 TN treated scr vs. TN treated TRIP13-sh1 in RPMI 8226. P<0.0001 scr vs. TN treated scr; P=0.0004 TRIP13-sh1 vs. TN treated TRIP13-sh1; P=0.0006 TN treated scr vs. TN treated TRIP13-sh1 in OCI-My5. Scale bar, 100 μm. (F) OCI-My5 cells with Scr or TRIP13-sh1 were treated with or without TN (30 nM) for 48 h, followed by assessment of apoptosis using flow cytometry. P<0.0001 scr vs. TN treated scr, TRIP13 sh1 vs. TN treated TRIP13-sh1, and TN treated scr vs. TN treated TRIP13-sh1. (G) RPMI 8226 and OCI-My5 cells with Scr, TRIP13-sh1, or TRIP13-sh2 were treated with or without different doses of TN for 48 h, after which the IC_{50} values of TN in these cells were determined by CCK-8 assay. (H) MM cells with Scr or TRIP13-sh1 were treated with TN (40 nM in RPMI 8226; 30 nM in OCI-My5) and BTZ (1.5 nM) alone or in combination for 48 h, followed by CCK-8 assay. P<0.0001of scr (TN vs. TN + BTZ, BTZ vs. TN + BTZ); P=0.849, P=0.0181 TRIP13-sh1 (TN vs. TN + BTZ, BTZ vs. TN + BTZ) in RPMI 8226 cells. P=0.0001, P<0.0001 scr (TN vs. TN + BTZ, BTZ vs. TN + BTZ); P=0.593, P=0.0253 TRIP13-sh1 (TN vs. TN + BTZ, BTZ vs. TN + BTZ) in OCI-My5 cells. n=3 independent experiments in (E-H). Statistical significance was assessed using one-way ANOVA followed by Tukey's honestly significant difference test in (E, F, and H). TN, triptonide; EV, empty vector; BTZ, bortezomib; MM, multiple myeloma; EdU, 5-Ethynyl-2'-deoxyuridine.

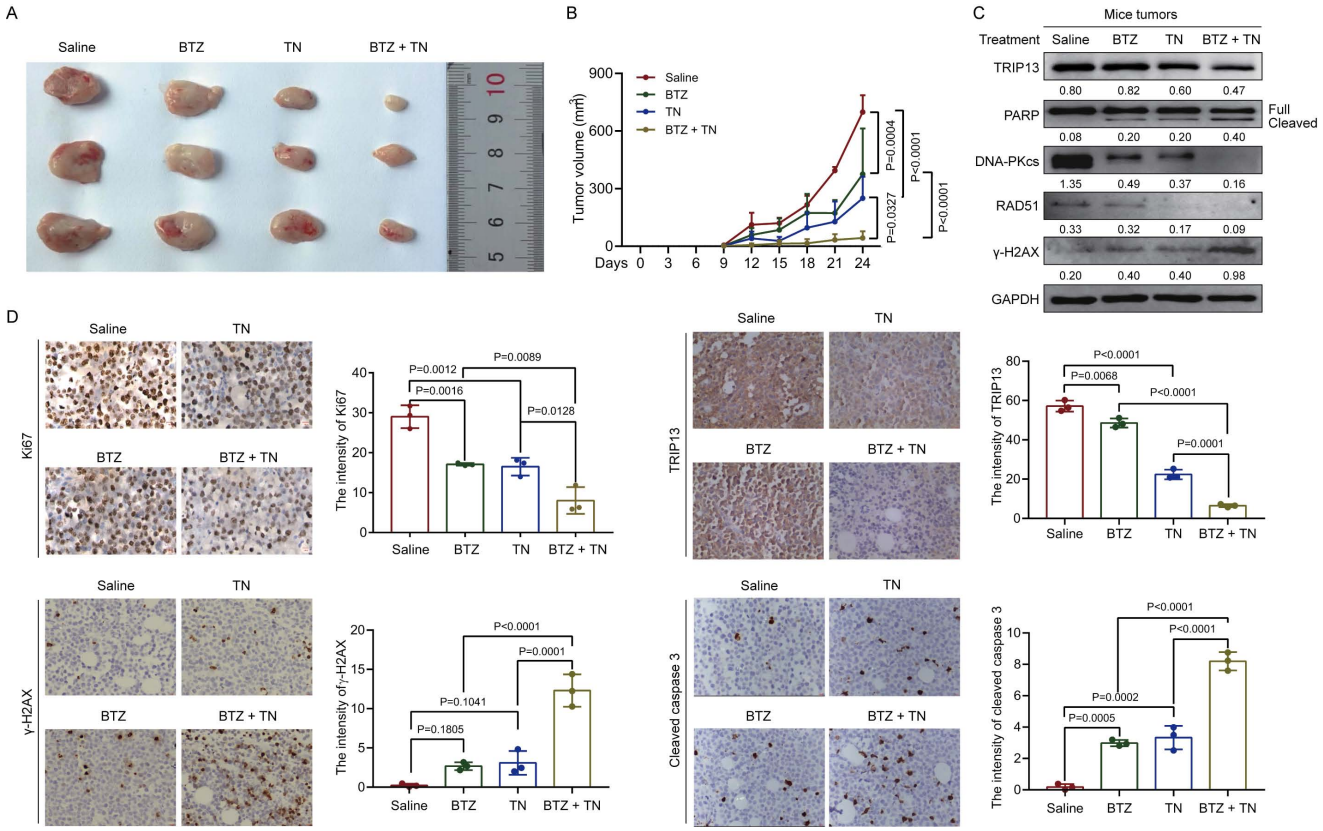

Figure 7. TN synergizes with BTZ to inhibit MM growth *in vivo*. (A) Tumor knots developed in NCG mice injected with OCI-My5 cells and treated with saline (n=3), TN (2.5 mg/kg) (n=3), BTZ (0.5 mg/kg) (n=3), or TN + BTZ (n=3). (B) Analysis of tumor volumes in those mice. P=0.0004, P<0.0001, P<0.0001 and P=0.0327 of tumor volumes (saline vs. BTZ, saline vs. TN, BTZ vs. BTZ + TN, and TN vs. BTZ + TN). (C) Western blot analysis of TRIP13, PARP, DNA-PKcs, RAD51, γ-H2AX and GAPDH in tumor knots derived from those mice. (D) IHC staining of Ki67, TRIP13, γ-H2AX and cleaved caspase 3 in tumor sections derived from those mice. P=0.0016, P=0.0068, P=0.1805 and P=0.0005 of Ki67, TRIP13, γ-H2AX and cleaved caspase 3 (saline vs. BTZ). P=0.0012, P<0.0001, P=0.1041 and P=0.0002 of Ki67, TRIP13, γ-H2AX and cleaved caspase 3 (saline vs. TN). P=0.0089, P<0.0001, P<0.0001 and P<0.0001 of Ki67, TRIP13, γ-H2AX and cleaved caspase 3 (BTZ vs. BTZ + TN). P=0.0128, P=0.0001, P=0.0001 and P<0.0001 of Ki67, TRIP13, γ-H2AX and cleaved caspase 3 (TN vs. BTZ + TN). Scale bar, 10 μm. Statistical significance was assessed using two-way repeated-measures ANOVA in (B); one-way ANOVA followed by Tukey's honestly significant difference test was applicated in (D). TN, triptonide; BTZ, bortezomib; MM, multiple myeloma; IHC, immunohistochemical.

to the TRIP13 protein, supported by a high binding affinity (-7.35 kcal/mol) and favorable binding energy (-37.89 kJ/mol; Fig. 5E-N). These findings indicated that TN interacts with TRIP13 and reduces its expression in MM cells. In addition, TN significantly suppressed TRIP13 expression and concurrently elevated γ-H2AX levels in primary MM cells (Fig. 5O). Notably, the combination of TN and BTZ synergistically decreased the levels of TRIP13, DNA-PKcs, and RAD51 in both RPMI 8226 and OCI-My5 cells (Fig. 5P). Therefore, TRIP13 may mediate the synergy between TN and BTZ in MM cells.

TN inhibits DNA repair and exerts synergistic effects with BTZ through targeting TRIP13. To define the role of TRIP13 in NHEJ, HR and the DNA damage response in MM cells, the present study overexpressed or knocked down TRIP13 and assessed DNA-PKcs, RAD51, and γ-H2AX by western blotting. TRIP13 overexpression increased DNA-PKcs and RAD51 while decreasing γ-H2AX; knockdown produced the opposite effects (Fig. 6A and B). TN suppressed DNA-PKcs and RAD51 and elevated γ-H2AX in TRIP13-overexpressing cells (Fig. 6C), but these effects were attenuated upon TRIP13 silencing (Fig. 6D), confirming that TN impairs DNA repair and amplifies DNA damage by targeting TRIP13. Given the association of TRIP13 with MM initiation, relapse and poor prognosis (22), and its emerging therapeutic relevance (42), whether TRIP13 loss rescues MM cells from TN was tested. EdU staining revealed higher proliferation (more EdU positive cells) in TN-treated, TRIP13-silenced compared control cells (Fig. 6E). Apoptosis was markedly reduced in TN-treated OCI-My5 cells after TRIP13 knockdown (Fig. 6F). TRIP13 silencing also increased TN's IC_{50} in both lines (Fig. 6G), indicating diminished sensitivity. Together, these data established TRIP13 as a key mediator of TN's anti-MM activity. Notably, TRIP13 knockdown markedly blunted the cytotoxic synergy of TN + BTZ (Fig. 6H). Thus, TRIP13 is essential for both the single-agent efficacy and the synergy with BTZ in MM by TN.

TN and BTZ synergistically inhibit MM progression in vivo. To assess the *in vivo* synergy of TN and BTZ against MM, OCI-My5 cells were implanted subcutaneously in immunodeficient NCG mice. At nine days later, mice were randomized into four groups and treated with saline, BTZ, TN, or TN + BTZ. Tumor volume and diameter were measured every three days in tumor-bearing mice using digital calipers (43). At the final measurement, the maximum tumor volume and diameter reached 800 mm^3 and 18 mm, respectively. After 24 h of

the final measurement, all mice were humanely sacrificed, and tumors were excised for subsequent analysis (Fig. 7A). The largest tumor diameter among the excised tumors was 21.5 mm, observed in the saline control group. As tumors naturally continued to grow in mice over the 24 h, the final measurements of tumor diameter and the excised tumors were slightly different. The combination group showed markedly slower tumor growth than either monotherapy group (Fig. 7B). Western blotting confirmed that TN downregulated TRIP13, DNA-PKcs and RAD51 while increasing γ-H2AX; the combination further elevated cleaved PARP and γ-H2AX beyond either drug alone (Fig. 7C), demonstrating enhanced DNA damage and apoptosis via TRIP13 suppression. Furthermore, IHC revealed lower Ki67 (a proliferation marker) and TRIP13, and higher γ-H2AX and cleaved caspase 3, in the combination group versus monotherapies (Fig. 7D). TN has shown safety in various preclinical studies (6,20). Here, no body weight loss occurred across groups (Fig. S5A), and hematoxylin and eosin (H&E) staining showed no histopathological abnormalities in kidney, lung, heart, or liver (Fig. S5B). Thus, TN is well-tolerated and effective in MM, and TN + BTZ is a promising therapeutic strategy.

Discussion

Although current treatment strategies have improved clinical outcomes for patients with MM, the disease remains an incurable hematological malignancy (44). The present study demonstrated that TN served as a potential targeted agent for MM treatment. Intriguingly, a synergistic effect was observed when TN was combined with BTZ across MM cell lines, primary MM cells, and MM mouse models.

TN exerts cytotoxic effects selectively on MM cell lines and primary MM cells, while exhibiting minimal toxicity toward B cell lines and primary non-MM cells. This selective cytotoxicity supports the potential of TN as a targeted therapeutic agent for MM. BTZ is a primary first-line therapeutic agent for MM (32). Combination therapies based on BTZ have substantially improved the survival outcomes of patients with MM (2,3). However, the clinical utility of BTZ is increasingly limited by the development of drug resistance (4) and adverse effects, such as peripheral neuropathy (45), thrombotic microangiopathy (46) and acute interstitial nephritis (32). The present study demonstrated that the combination of TN and BTZ synergistically inhibits MM cells both *in vitro* and *in vivo*. This combination regimen may overcome BTZ resistance and reduce the required dosage of BTZ, thereby minimizing associated side effects. Therefore, TN plus BTZ represents a promising therapeutic strategy for the treatment of MM.

BTZ induces DNA damage by elevating reactive oxygen species (ROS) levels in MM cells (41), while TN promotes DNA damage by inhibiting DNA repair. These distinct mechanisms synergize to enhance DNA damage, underpinning the combined effect of TN and BTZ. Yang *et al* (47) reported that TN inhibits the NHEJ pathway via the lipogenic LXR-SREBF1 axis, while the present study showed that TN suppresses both NHEJ and HR pathways by targeting TRIP13, a key DNA repair regulator linked to BTZ resistance in MM (22,42). The present study showed that TN directly binds TRIP13 and reduces its expression, identifying it as a novel TRIP13 inhibitor. TRIP13 silencing partly attenuates TN-induced apoptosis and DNA damage and abolishes the synergistic anti-MM effect of TN and BTZ. TRIP13 plays a critical role in mediating BTZ resistance and elevated TRIP13 expression is associated with poor prognosis in patients with MM (22). Impairing TRIP13-mediated DNA repair increases DNA damage and exerts potent anti-MM activity (48). Therefore, TN enhances DNA damage by suppressing TRIP13, contributing to synergy with BTZ. Together, TN in combination with BTZ represents a promising therapeutic strategy for MM.

Acknowledgements

The authors would like to thank Professor Wen Zhou from Central South University School of Basic Medical Sciences (Hunan, China) for providing MM cell lines. The authors also thank Easy2MD (https://github.com/easy2md) program for the analysis of molecular simulation data.

Funding

The present study was supported by grants from the Natural Science Foundation of Hunan Province (grant nos. 2023JJ10036 and 2026JJ82105); PhD Scientific Research Start-up Fund of the University of South China (grant no. 200XQD075); Scientific Research Project of Hunan Department of Education (grant no. 22B0452); Innovation Platform Open Fund Project of Department of Education of Hunan Province (grant no. 20K110). National College Student Innovation and Entrepreneurship Training Program (grant no. S202410555226).

Availability of data and materials

The raw data of RNA-sequencing reported in the present study has been deposited in the public database of Genome Sequence Archive (GSA) in National Genomics Data Center under the accession number HDAC007930, which is accessible at https://ngdc.cncb.ac.cn/gsa-human/browse/dac/HDAC007930. The data generated in the present study may be requested from the corresponding author.

Authors' contributions

JX, FH, JLi and XZ designed the present study and drafted the article. FH, LP, HZ, ML and RG performed experiments, collected data and conducted initial data analysis. SW, YC, JLi, LP and CL collected clinical specimens and analyzed clinical data. RT, ZL, LZ, XZ, QL, WC and JLiu participated in experiment operation and data analysis. JX and FH confirm the authenticity of all the raw data. All authors read and approved the final manuscript.

Ethics approval and consent to participate

Written informed consent were obtained from all the patients who were involved in the study, and the research protocol was approved by the Ethics Committee of the Hengyang Medical School of University of South China (approval no. 20250033). Animal studies were approved by the Animal Ethics

Committee of the Hengyang Medical School of University of South China (approval no. USC2024XS052).

Patient consent for publication

Not applicable

Competing interests

The authors declare that they have no competing interests.

References

1. Malard F, Neri P, Bahlis NJ, Terpos E, Moukalled N, Hungria VTM, Manier S and Mohty M: Multiple myeloma. Nat Rev Dis Primers 10: 45, 2024.
2. Durie BGM, Hoering A, Abidi MH, Rajkumar SV, Epstein J, Kahanic SP, Thakuri M, Reu F, Reynolds CM, Sexton R, *et al*: Bortezomib with lenalidomide and dexamethasone versus lenalidomide and dexamethasone alone in patients with newly diagnosed myeloma without intent for immediate autologous stem-cell transplant (SWOG S0777): A randomised, open-label, phase 3 trial. Lancet 389: 519-527, 2017.
3. Lakshman A, Singh PP, Rajkumar SV, Dispenzieri A, Lacy MQ, Gertz MA, Buadi FK, Dingli D, Hwa YL, Fonder AL, *et al*: Efficacy of VDT PACE-like regimens in treatment of relapsed/refractory multiple myeloma. Am J Hematol 93: 79-186, 2018.
4. Li F, Liu J and Fu Y: Acquired bortezomib resistance in multiple myeloma: From mechanisms to strategy. Curr Treat Options Oncol 25: 1354-1365, 2024.
5. Chang Z, Qin W, Zheng H, Schegg K, Han L, Liu X, Wang Y, Wang Z, McSwiggin H, Peng H, *et al*: Triptonide is a reversible non-hormonal male contraceptive agent in mice and non-human primates. Nat Commun 12: 1253, 2021.
6. Song J, He GN and Dai L: A comprehensive review on celastrol, triptolide and triptonide: Insights on their pharmacological activity, toxicity, combination therapy, new dosage form and novel drug delivery routes. Biomed Pharmacother 162: 114705, 2023.
7. Xiang S, Zhao Z, Zhang T, Zhang B, Meng M, Cao Z and Zhou Q: Triptonide effectively suppresses gastric tumor growth and metastasis through inhibition of the oncogenic Notch1 and NF-κB signaling pathways. Toxicol Appl Pharmacol 388: 114870, 2020.
8. Zhang M, Tan S, Yu D, Zhao Z, Zhang B, Zhang P, Lv C, Zhou Q and Cao Z: Triptonide inhibits lung cancer cell tumorigenicity by selectively attenuating the Shh-Gli1 signaling pathway. Toxicol Appl Pharmacol 365: 1-8, 2019.
9. Ma J, Zheng L, Fang S, Yang W, Ding Y, Wang M, Chen J, Weng Q, Yao Z, Jiang C, *et al*: Triptonide stabilizes BIM to enhance oxaliplatin-induced ferroptosis and apoptosis in colorectal cancer. Transl Oncol 60: 102491, 2025.
10. Lou R, Yang T, Zhang X, Gu J, Xue L, Gan D, Li H, Li Q, Chen Y and Jiang J: Triptonide induces apoptosis and inhibits the proliferation of ovarian cancer cells by activating the p38/p53 pathway and autophagy. Bioorg Med Chem 110: 117788, 2024.
11. Zhang M, Meng M, Liu Y, Qi J, Zhao Z, Qiao Y, Hu Y, Lu W, Zhou Z, Xu P and Zhou Q: Triptonide effectively inhibits triple-negative breast cancer metastasis through concurrent degradation of Twist1 and Notch1 oncoproteins. Breast Cancer Res 23: 116, 2021.
12. Tan S, Zhao Z, Qiao Y, Zhang B, Zhang T, Zhang M, Qi J, Wang X, Meng M and Zhou Q: Activation of the tumor suppressive hippo pathway by triptonide as a new strategy to potently inhibit aggressive melanoma cell metastasis. Biochem Pharmacol 185: 114423, 2021.
13. Xu Y, Wang P, Li M, Wu Z, Li X, Shen J and Xu R: Natural small molecule triptonide inhibits lethal acute myeloid leukemia with FLT3-ITD mutation by targeting Hedgehog/FLT3 signaling. Biomed Pharmacother 133: 111054, 2021.
14. Zhang B, Meng M, Xiang S, Cao Z, Xu X, Zhao Z, Zhang T, Chen B, Yang P, Li Y and Zhou Q: Selective activation of tumor-suppressive MAPKP signaling pathway by triptonide effectively inhibits pancreatic cancer cell tumorigenicity and tumor growth. Biochem Pharmacol 166: 70-81, 2019.
15. Ju J, Xu N, Li B, Shi D, Cai J, Zheng Q, Ye L, Zhang S and Wang C: Triptonide facilitates autophagy-mediated apoptosis in esophageal squamous cell carcinoma by targeting the AMPK-mTOR-ULK1 axis. Acta Biochim Biophys Sin (Shanghai) 57: 1611-1624, 2025.
16. Wang W, Zhao X, Zhou J and Li H: A novel antitumor mechanism of triptonide in colorectal cancer: Inducing ferroptosis via the SLC7A11/GPX4 axis. Funct Integr Genomics 24: 126, 2024.
17. Pan Y, Meng M, Zheng N, Cao Z, Yang P, Xi X and Zhou Q: Targeting of multiple senescence-promoting genes and signaling pathways by triptonide induces complete senescence of acute myeloid leukemia cells. Biochem Pharmacol 126: 34-50, 2017.
18. Zheng Z, Chen Y, Wang C, Li L and Tan B: Triptolide induces immunogenic cell death in cervical cancer cells via ER stress and redox modulation. Am J Cancer Res 15: 69-83, 2025.
19. Li X, Chen L, Yan Z, Xu T and Zhao Y: Triptonide suppresses the FOXK1/AKT2 axis to reverse malignant phenotype and improve cisplatin efficacy in esophageal squamous cell carcinoma. Genes Genomics 47: 1343-1353, 2025.
20. Yang P, Dong F and Zhou Q: Triptonide acts as a novel potent anti-lymphoma agent with low toxicity mainly through inhibition of proto-oncogene Lyn transcription and suppression of Lyn signal pathway. Toxicol Lett 278: 9-17, 2017.
21. Wang K, Sturt-Gillespie B, Hittle JC, Macdonald D, Chan GK, Yen TJ and Liu ST: Thyroid hormone receptor interacting protein 13 (TRIP13) AAA-ATPase is a novel mitotic checkpoint-silencing protein. J Biol Chem 289: 23928-23937, 2014.
22. Li C, Xia J, Franqui-Machin R, Chen F, He Y, Ashby TC, Teng F, Xu H, Liu D, Gai D, *et al*: TRIP13 modulates protein deubiquitination and accelerates tumor development and progression of B cell malignancies. J Clin Invest 131: e146893, 2021.
23. Banerjee R, Russo N, Liu M, Basrur V, Bellile E, Palanisamy N, Scanlon CS, van Tubergen E, Inglehart RC, Metwally T, *et al*: TRIP13 promotes error-prone nonhomologous end joining and induces chemoresistance in head and neck cancer. Nat Commun 5: 4527, 2014.
24. Clairmont CS, Sarangi P, Ponnienselvan K, Galli LD, Csete I, Moreau L, Adelmant G, Chowdhury D, Marto JA and D'Andrea AD: TRIP13 regulates DNA repair pathway choice through REV7 conformational change. Nat Cell Biol 22: 87-96, 2020.
25. Zhang H, Wei Z, Han S and Zhao S: Triptonide inhibits the progression of oral squamous cell carcinoma by suppressing the TRIP13/c-Myc axis. Neoplasma 72: 36-47, 2025.
26. Xu L, Wang Y, Wang G, Guo S, Yu D, Feng Q, Hu K, Chen G, Li B, Xu Z, *et al*: Aberrant activation of TRIP13-EZH2 signaling axis promotes stemness and therapy resistance in multiple myeloma. Leukemia 37: 1576-1579, 2023.
27. Shi M, Shen N, Liu X, Yu J, Shen X, Chen Y, Xia Y and Chen L: Exosome-transmitted HSPA9 facilitates bortezomib resistance by targeting TRIP13/USP1 signaling in multiple myeloma. Cell Commun Signal 23: 152, 2025.
28. Xia J, Zhang J, Wu X, Du W, Zhu Y, Liu X, Liu Z, Meng B, Guo J, Yang Q, *et al*: Blocking glycine utilization inhibits multiple myeloma progression by disrupting glutathione balance. Nat Commun 13: 4007, 2022.
29. Zhang Y, He F, Hu W, Sun J, Zhao H, Cheng Y, Tang Z, He J, Wang X, Liu T, *et al*: Bortezomib elevates intracellular free Fe^{2+} by enhancing NCOA4-mediated ferritinophagy and synergizes with RSL-3 to inhibit multiple myeloma cells. Ann Hematol 103: 3627-3637, 2024.
30. Yang X, Zhang J, Ma J, Huang J, Wang P, Wang F and Tang X: Integrative investigation on the mechanisms of modified Zuojin pill (SQQT) in ameliorating gastric metaplasia. J Ethnopharmacol 346: 119643, 2025.
31. Livak KJ and Schmittgen TD: Analysis of relative gene expression data using real-time quantitative PCR and the 2(-delta delta C(T)) method. Methods 25: 402-408, 2001.
32. Sogbein O, Paul P, Umar M, Chaari A, Batuman V and Upadhyay R: Bortezomib in cancer therapy: Mechanisms, side effects, and future proteasome inhibitors. Life Sci 358: 123125, 2024.
33. Mateos MV, Dimopoulos MA, Cavo M, Suzuki K, Jakubowiak A, Knop S, Doyen C, Lucio P, Nagy Z, Kaplan P, *et al*: Daratumumab plus bortezomib, melphalan, and prednisone for untreated myeloma. N Engl J Med 378: 518-528, 2018.

34. Mushtaq A, Cheema AY, Ali HM, Shatnawi Y, Ashruf O, Ahmad EN, Lytvynova O, Munir M, Asif MA, Ahmad M, *et al*: Management of relapsed refractory multiple myeloma: Evidence-based guide to community oncologists. Blood Rev 74: 101339, 2025.
35. Chou TC: Drug combination studies and their synergy quantification using the Chou-Talalay method. Cancer Res 70: 440-446, 2010.
36. Gao B, Chen J, Han B, Zhang X, Hao J, Giuliano AE, Cui Y and Cui X: Identification of triptonide as a therapeutic agent for triple negative breast cancer treatment. Sci Rep 11: 2408, 2021.
37. Mustafa M, Ahmad R, Tantry IQ, Ahmad W, Siddiqui S, Alam M, Abbas K, Moinuddin, Hassan MI, Habib S, *et al*: Apoptosis: A comprehensive overview of signaling pathways, morphological changes, and physiological significance and therapeutic implications. Cells 13: 1838, 2024.
38. Elango R, Panday A, Lach FP and Willis NA: DNA double-strand break repair-pathway choice in somatic mammalian cells. Nat Rev Mol Cell Biol 20: 698-714, 2019.
39. Tan J, Sun X, Zhao H, Guan H, Gao S and Zhou PK: Double-strand DNA break repair: Molecular mechanisms and therapeutic targets. MedComm (2020) 4: e388, 2023.
40. Siegel SR, Ulrich M and Logue SF: Comparison qPCR study for selecting a valid single copy gene for measuring absolute telomere length. Gene 860: 147192, 2023.
41. Yin L, Kufe T, Avigan D and Kufe D: Targeting MUC1-C is synergistic with bortezomib in downregulating TIGAR and inducing ROS-mediated myeloma cell death. Blood 123: 2997-3006, 2014.
42. Jacob Bunu S, Cai H, Wu L, Zhang H, Zhou Z, Xu Z, Shi J and Zhu W: TRIP13-a potential drug target in cancer pharmacotherapy. Bioorg Chem 151: 107650, 2024.
43. Wang X, Zhou D, Jin C, Shi Z, Wen D and Bi L: Establishment of patient-derived xenograft models in Chinese patients with multiple myeloma: Insights into therapeutic responsiveness and molecular subtyping. Transl Oncol 56: 102385, 2025.
44. Elbezanti WO, Challagundla KB, Jonnalagadda SC, Budak-Alpdogan T and Pandey MK: Past, present, and a glance into the future of multiple myeloma treatment. Pharmaceuticals (Basel) 16: 415, 2023.
45. Velasco R, Alberti P, Bruna J, Psimaras D and Argyriou AA: Bortezomib and other proteosome inhibitors-induced peripheral neurotoxicity: From pathogenesis to treatment. J Peripher Nerv Syst 24 (Suppl 2): S52-S62, 2019.
46. Deng Z, Wang S and Wang C: Proteasome inhibitor-associated thrombotic microangiopathy: A real-world retrospective and pharmacovigilance database analysis. Support Care Cancer 33: 184, 2025.
47. Yang B, Zhang B, Cao Z, Xu X, Huo Z, Zhang P, Xiang S, Zhao Z, Lv C, Meng M, *et al*: The lipogenic LXR-SREBF1 signaling pathway controls cancer cell DNA repair and apoptosis and is a vulnerable point of malignant tumors for cancer therapy. Cell Death Differ 27: 2433-2450, 2020.
48. Chang S, Xiao W, Xie Y, Xu Z, Li B, Wang G, Hu K, Zhang Y, Zhou J, Song D, *et al*: TI17, a novel compound, exerts anti-MM activity by impairing Trip13 function of DSBs repair and enhancing DNA damage. Cancer Med 12: 21321-21334, 2023.